Cantore, L., Oth, A., Parolai, S., Bindi, D. (2011): Attenuation, source parameters and site effects in the Irpinia-Basilicata region (southern Apennines, Italy). - Journal of Seismology, 15, 2, 375-389

DOI: 10.1007/s10950-011-9230-2

Attenuation, source parameters and site effects in the Irpinia-Basilicata region (southern Apennines, Italy)

Luciana Cantore[1], Adrien Oth[2,*], Stefano Parolai[3], Dino Bindi[4]

J. Seismol., 15(2), 375-389

doi: 10.1007/s10950-011-9230-2

(preprint)

1) Dipartimento di Scienze Fisiche, Universita degli Studi di Napoli Federico II, Naples I-80125, Italy.
2) European Center for Geodynamics and Seismology, rue Josy Welter 19, L-7256 Walferdange, Luxembourg
3) Helmholtz Centre Potsdam, GFZ German Research Centre for Geosciences, Earthquake Risk and Early Warning Section, Telegrafenberg, D-14473 Potsdam, Germany
4) Helmholtz Centre Potsdam, GFZ German Research Centre for Geosciences, Centre for Disaster Management and Risk Reduction Technology (CEDIM), Telegrafenberg, D-14473 Potsdam, Germany

Corresponding author, adrien.oth@ecgs.lu

ABSTRACT

We derive S-wave attenuation characteristics, earthquake source parameters and site amplification functions at seismic stations used for earthquake early warning in the Irpinia-Basilicata region, using non-parametric spectral inversion of seismograms from 49 local events with M_L=1.5-3.1. We obtain relatively low Q-values (Q_0=28 at a frequency of 1 Hz) in conjunction with a strong frequency-dependence (close to linear). The source spectra can be satisfactorily modeled using the omega-square model, with stress drops ranging between 0.01-2 MPa, and in the narrow magnitude range available for analysis, the source spectra seem to scale self-similarly. The local magnitude M_L shows a linear correlation with moment magnitude M_W, however with a systematic underestimation by about 0.5 magnitude units. The results obtained in this work provide important insights into the ground motion characteristics that are required for appropriate seismic hazard assessment and are of practical relevance for a suite of applications, such as the calibration of ground-motion prediction equations or the correction for site amplification in earthquake early warning and rapid calculation of shake-maps for seismic emergency management.

INTRODUCTION

The southern Apennines represent an active tectonic region within Italy that accommodates differential motions between the Adria and Tyrrhenian microplates, responsible for almost all of the seismicity occurring in this region. Recent in situ stress data research (Montone et al., 2004) and seismological data analysis indicate that an extensional stress regime is prevalent in the southern Apennines, and that the seismic activity is confined to the narrow upper-crustal seismic zone. In particular, two main

clusters of crustal earthquakes may be identified: the westernmost cluster with shallow earthquakes (depths < 20 km) along the axis chain (Irpinia area) and the easternmost cluster with deeper earthquakes (about 20-40 km) located on the outer margin of the chain (Potentino area) and the foredeep. The earthquakes in these two clusters show different focal mechanisms indicating a pure extensional regime to the west (Irpinia) and a strike-slip regime to the east (Potentino).

During the last century, three large earthquakes with magnitudes greater than 6 have occurred in the Irpinia-Basilicata region: the 1930 M 6.7 Irpinia earthquake (Emolo et al., 2004), the 1962 M 6.2 Irpinia earthquake (Westaway, 1987), and the 1980 M 6.9 Irpinia-Basilicata earthquake (Westaway and Jackson, 1987; Bernard and Zollo, 1989; Pantosti and Valensise, 1990). Particularly the 1980 Irpinia-Basilicata earthquake caused catastrophic damage throughout the region, resulting in about 3,000 fatalities. Today, seismicity is mainly concentrated within or close to the fault system associated with the 1980 Irpinia-Basilicata earthquake and several moderate-size events occurred in recent years, such as the 1990 and 1991 Potenza earthquakes (M 5.4 and 5.1, within the deeper strike-slip zone) and the 1996 event (M 4.9). This recent seismic activity provides clear indications that the Irpinia-Basilicata region still represents a region of high seismic risk, now and in the future (Cinti et al., 2004).

In response to this threat, an earthquake early warning system prototype is in development in the Campania-Lucania region, the core of which is made up of the dense Irpinia Seismic Network (ISNet) recently installed along the southern Apennines chain (Figure 1). It is equipped with sensors that can provide high-quality recordings of both weak motions from small-magnitude events as well as strong ground shaking, thus enabling scientists to retrieve information about the rupture processes and to obtain insights into the

scaling relationships between small and large events (Convertito et al., 2009). The network consists of 27 seismic instruments and covers an area of approximately 100x70 km^2 and has been especially designed to provide optimal coverage of the active fault system that generated the November 23 1980 Irpinia earthquake (Weber et al., 2007). Each station is equipped with a strong-motion accelerometer (Guralp CMG-5T) and a short period three-component seismometer (Geotech S13-J with natural period of 1 second), thus covering the entire necessitated dynamic recording range.

The ISNet seismic network was installed with the purpose of monitoring in real-time the potential source region of destructive earthquakes (i.e., the region around the source zone of the 1980 event) that, beyond the evident threat that these pose within the immediate source area, also represent a serious danger to the city of Naples and the densely populated coast. Thus, it is of utmost importance to provide the best possible characterization of the seismic recordings obtained at this local-scale network. One major aim of the work presented in this article is therefore to characterize the frequency-dependent site response for the ISNet stations by applying the generalized inversion technique (GIT) to the Fourier amplitude spectra (FAS) of ground motion. In addition to the information on site response, this technique provides us with insights into seismic attenuation characteristics within the area covered by the network as well as source spectra of the utilized events, parameters that are of considerable importance to better understand seismic ground motions in the area.

We first provide an overview of the dataset and the applied methodology, followed by a discussion of seismic attenuation and, in particular, its frequency-dependence. From the source spectra, we investigate the scaling characteristics in the available magnitude range, derive the stress drops of the events and discuss the scaling relation between local and moment magnitude. Finally, the site response functions for the ISNet stations are

discussed and compared to the H/V spectral ratios calculated directly from the ground motion spectra.

DATASET

Seismograms from 49 local earthquakes that occurred between February 2006 and November 2008 recorded by the short-period sensors of 22 ISNet stations constitute the basis of our analysis. Data were recorded with a sampling rate of 125 samples per second, and we only considered events and stations with at least 3 available recordings. For most earthquakes and stations, however, more than 5 respectively 10 records could be used. Figure 2 shows the station locations, the epicenters of the selected events and the source-station travel paths, which together show a satisfactory coverage of the area inside the network. The hypocentral distances range from 5 to 83 km with best coverage between 10 to 65 km (Figure 3a), and the focal depths of the events are all shallower than 30 km. The covered magnitude range is rather narrow ($1.5<M_L<3.1$) (Figure 3b), with the largest number of events in the range M_L=1.5-2.5.

The records were baseline corrected, the effect of instrumental response was removed and the resulting seismograms were finally high-pass filtered applying a four-pole Butterworth filter with corner frequency 0.2 Hz. For the purpose of our analysis, only the S-wave portions of the records were used. Time windows starting 1 sec before the S-wave onset (picked on the horizontal components) with a length of 5 sec were extracted. Before calculation of the FAS, the beginning and end of each window were tapered with a 5% cosine window and the computed spectra were smoothed around 40 frequency points equally spaced on logarithmic scale between 1 and 30 Hz using the smoothing function proposed by Konno and Ohmachi (1998) with b = 40. Pre-event noise windows with the same length as the S-wave windows were used to compute the signal-to-noise (SNR) ratio

and at each frequency point, only records with a SNR higher than 3 were considered. Due to this SNR-based selection, the number of data points entering the inversion is slightly different at each frequency. Finally, the horizontal- component spectra were combined to their root-mean-square (rms) average.

METHODS

In order to separate source spectra, attenuation characteristics and site response functions from one another, we applied a two-step non-parametric spectral inversion scheme as originally proposed by Castro et al. (1990) (termed below as generalized inversion technique, GIT) to the velocity spectra of the ISNet S-wave records. We applied the GIT inversion both to horizontal and vertical components and compared the site response functions obtained by the GIT inversion with the H/V ratios calculated directly from the observed ground motion spectra at each station.

Generalized inversion technique (GIT)

Since the applied GIT approach is commonly used in the literature (e.g. Castro et al., 1990; Parolai et al., 2000, 2004; Oth et al., 2008, 2009), we limit our discussion on the methodology to the basic concept and refer the reader to the latter publications for the details. We followed the two-step procedure introduced by Castro et al. (1990): in the first step, the dependence of the spectral amplitudes on distance for a given frequency *f* is given by

$$U_{ij}(f, r_{ij}) = A(f, r_{ij}) \cdot \hat{S}_j(f), \quad (1)$$

where $U_{ij}(f, r_{ij})$ represents the observed spectral amplitude at the i-th station resulting from the j-th earthquake, r_{ij} is the source-site distance, $A(f, r_{ij})$ is the non-parametric attenuation function, and $\hat{S}_j(f)$ is a scalar factor that depends on the size of the j-th source. In this

model, the functional form of $A(f, r_{ij})$ is not pre-defined and implicitly includes all effects causing attenuation along the travel path (geometrical spreading, anelasticity, scattering, etc.). Since the properties causing attenuation within the Earth's crust are thought to vary slowly with distance, $A(f, r_{ij})$ is constrained to be a smooth decaying function with distance r and to take the value $A(f, R_0) = 1$ at a specific reference distance R_0 (5 km in our case). Site effects are not included in the formulation given by equation (1) and are supposed to be primarily absorbed into the residuals of the observed ground motion spectra from this parameterization.

For N spectral records, equation (1) represents a linear system of N equations, which is formed for each frequency analyzed by taking the logarithm. The system of equations is solved using singular value decomposition (Menke, 1989), providing us with discretized (in bins of 2 km) attenuation functions $A(f, r_{ij})$ and the source scaling factors.

Estimates of the quality factor can be obtained through fitting a parametric model to $A(f, r)$:

$$A(f,r) = G(r)\exp\left(-\frac{\pi f r}{Q(f)v_S}\right). \quad (2)$$

Herein, $Q(f)$ is the S-wave quality factor, v_S the average shear wave velocity and $G(r)$ represents the geometrical spreading function. Since at distances larger than 70 km the attenuation functions are only constrained by very few data points, we only used the attenuation functions within distances lower than 70 km to derive $Q(f)$, setting the geometrical spreading function to $G(r)=5/r$. From equation (2), $Q(f)$ can be evaluated from the slope of a linear least-squares fit to log $A(f,r)$-log $G(r)$ versus distance. Finally, we investigate the frequency dependence of Q assuming a model of the form $Q(f) = Q_0 f^N$.

After the attenuation functions $A(f, r_{ij})$ have been determined, the spectral amplitudes at each frequency are corrected for the effect of seismic attenuation and in the second inversion step, the corrected spectra are separated into source and site effects (Andrews, 1986):

$$R_{ij}(f) = S_j(f) \cdot Z_i(f). \tag{3}$$

Here, $R_{ij}(f) = U_{ij}(f, r_{ij}) / A(f, r_{ij})$ are the residual spectral amplitudes after correction for path effects, $S_j(f)$ is the source spectrum of the j-th earthquake, and $Z_i(f)$ the site amplification function at the i-th station. Equation (3) can be linearized as well by applying the logarithm.

As noted by Andrews (1986), equation (3) still contains one undetermined degree of freedom due to the linear dependence between site and source terms. This degree of freedom must be fixed by setting a reference condition either for at least one source or one site in the dataset. Usually, the site response of a rock site is fixed to one (respectively zero in $\log_{10}$), irrespective of frequency, or the average site response at a set of competent sites is set to unity.

We solved the second inversion by constraining the logarithm of the site amplification of a reference site to zero. We adopted station AND3 as the reference site because it is located on outcropping bedrock and the H/V ratio at this station is flat and almost equal to one over the entire analyzed frequency range (Figure 4), except at the lowest frequencies where there is a slight increase to a factor of about two. In order to evaluate the stability of the solution and estimate standard errors for the model parameters, we performed 200 bootstrap inversions (Efron and Tibshirani, 1994) for each of the 40 frequency points following the same procedure as used by Parolai et al. (2000, 2004) and

Oth et al. (2008, 2009). From the 200 bootstrap samples, the mean and standard error were calculated for each model parameter.

H/V ratios of earthquake data

The GIT site responses have been compared with those calculated by horizontal-to-vertical (H/V) ratios derived from earthquake data. The H/V method, originally introduced by Nakamura (1989) to interpret microtremor recordings, has become a very popular tool in site response estimation in recent years. Lermo and Chavez-Garcia (1993) first applied this technique to the S-wave part of earthquake recordings as well. The H/V method, in analogy to the so-called receiver-function technique used to investigate the crustal and upper mantle structures from teleseismic records (Langston, 1979), assumes that the vertical component of ground motion is mainly controlled by source and attenuation effects and is not very sensitive to local site amplification. Thus, by deconvolving, or dividing in the frequency domain, the vertical component from the horizontal one, an estimate of the site response function can be obtained. Because the S-wave amplification at the surface depends on the angle of incidence (Lermo and Chavez-Garcia, 1993), it is necessary to average over a sufficient number of events distributed around the station of interest with good azimuthal and distance coverage in order to obtain stable estimates (Parolai et al., 2004).

Generally, comparisons of site response functions obtained with different techniques (e.g., Field and Jacob, 1995; Bonilla et al., 1997; Parolai et al., 2004) have shown that the H/V method provides a good estimate of the fundamental frequency of resonance, but underestimates the level of amplification with respect to the GIT. Recently, Parolai and Richwalski (2004) showed that the observed differences in the estimated amplifications obtained applying different techniques could be linked to S-P conversions at the bottom of the soft layer in the case of high impedance contrasts.

RESULTS

Attenuation characteristics

The obtained non-parametric attenuation functions at all 40 frequency points are depicted in Figure 5a, color-coded with respect to their frequency, while in Figure 5b, two of the attenuation curves are depicted together with their estimated standard deviation from the bootstrap analysis. The latter plot shows that in general the attenuation curves are well constrained. The functions depict a relatively simple shape, being all monotonically decaying with a change in the rate of amplitude decay for hypocentral distances between 20 and 50 km at higher frequencies. Below 20 km distance, the high frequencies show a stronger decay with distance, while between 20 and 50 km, the slope of the attenuation curves adjusts to be very similar for almost the entire frequency band.

Figure 6 shows the values of *Q(f)* estimated for all frequencies using equation (2) (the vertical error bars indicate the regressional error of fit) and the least-squares fit of a relation of the form $Q(f) = Q_0 f^N$ obtained with these values (solid black line). As can be seen from Figure 6, the frequency-dependence of *Q(f)* can be well approximated with a power-law dependency given as:

$$Q(f) = 28.3 f^{0.87}. \quad (4)$$

We thus find a rather strong frequency-dependence of the quality factor in the region. Other models derived for different regions in Italy, including southern Italy where the region under investigation by this study is located, are indicated in Figure 6 as well (within the overlap of the frequency range of their validity and the range 1-30 Hz of our study, see also Table 1). In particular, Castro et al. (2004b) derived the relationship $Q(f) = 32.1 f^{1.7}$ from a dataset of 32 earthquakes recorded at 4 stations of the Basilicata seismic network.

They obtained a much stronger frequency-dependence with N>1, while in contrast the value of Q_0 is rather close to the one found here. Castro et al. (2008) corroborated the results of Castro et al. (2004b), using a significantly extended dataset from the same seismic network. They furthermore used a more sophisticate analysis procedure on their non-parametric attenuation curves, providing separate estimations of upper und lower crustal attenuation characteristics in the frequency range 1-25 Hz. Assuming body-wave geometrical spreading ($\propto 1/r$) over the first 50 km, they obtained the Q-model $Q(f) = 18.8 f^{1.7}$ for the upper crust (depth < 13 km). While this frequency dependence is identical to one obtained by Castro et al. (2004b), attenuation is slightly larger at all frequencies due to the lower Q_0 value (18.8 vs. 32.1). Considering however the typical uncertainty ranges in determining such Q(f) models, the results of both studies are highly consistent with one another, and we only list the result of Castro et al. (2004b) in Table 1 and Figure 6. Another study covering the region of interest investigated coda-Q in the frequency range 1-12 Hz (Bianco et al., 2002) and the authors found from a multi lapse time window analysis that intrinsic Q seems to dominate with respect to scattering Q in the area. Other Q-models have been reported for different regions of Italy by Rovelli et al. (1988), Malagnini et al. (2000) and Castro et al. (2004a,b), and the one that matches our results most closely is the model for Umbria given by Castro et al. (2004a), with a frequency-dependence N=1.2. It is important to point out that due to the trade-off between Q and the geometrical spreading function, a reliable comparison between the different models only makes sense if the estimates of Q are made using similar geometrical spreading functions. Moreover, it should be noted that the data used to retrieve the attenuation models listed in Table 1 sample different frequency bands and different crustal volumes. The studies by Malagnini et al. (2000) and Rovelli et al. (1988) sample for

instance large regions such as the entire Apennines or the entirety of southern Italy. In contrast, our results are related to a small area limited by the extent of the ISNet network, and also Bianco et al. (2002) analyzed data from a much larger area surrounding the ISNet network. This limitation of our study to the small region covered by the ISNet network can however also be seen as an advantage in the sense that with the derived attenuation functions, we provide a means for reliable and consistent attenuation correction for events occurring in close proximity or within the network, avoiding a bias in source parameter or site response estimation due to inappropriate attenuation correction.

Source spectra

In order to remove the undetermined degree of freedom when separating source spectra and sites response from the attenuation-corrected spectral amplitudes as described by equation (3), we fixed the site response at the reference station AND3 to unity, irrespective of frequency. Since with the non-parametric attenuation functions discussed above we can only correct for attenuation up the reference distance of 5 km (i.e. the lowest distance in our dataset), the obtained source spectra from the second inversion step are also given at the reference distance of 5 km.

We did not include a term accounting for potential high-frequency decay due to the exponential κ-operator (Anderson and Hough, 1984) in the reference condition, and it may therefore be the case that some high-frequency decay due to near-surface high-frequency diminution at the reference site is systematically shifted into the source spectra. In order to investigate this issue, we plot the source spectra in acceleration (Figure 7a) and visually checked the high-frequency part of the spectra. As can be seen from Figure 7a, the acceleration source spectra generally show a clear plateau-like structure at highest frequencies, as would be expected in the case the ω^2-model (Brune, 1970, 1971) is valid.

Thus we cannot see any clear indication that a systematic high-frequency decay is moved into the source contributions. There is one systematic through appearing in the source spectra at a frequency of about 22-23 Hz, which may be due to an amplification effect at the reference station not accounted for in the inversion constraint.

In order to derive the source parameters (i.e. seismic moments and corner frequencies) of the 49 earthquakes in our dataset, we fitted the ω^2-model to the inverted source spectra (in acceleration, using the results from the horizontal component inversion) using non-linear least squares:

$$S(f) = (2\pi f)^2 \cdot \frac{R^{\theta\varphi} VF}{4\pi\rho v_S^3 R_0} \cdot M_0 \cdot \left[1 + \frac{f^2}{f_C^2}\right]^{-1}, \quad (5)$$

where $R^{\theta\varphi}$ is the average radiation pattern set to 0.55, $V=1/\sqrt{2}$ accounts for the separation of S-wave energy on two horizontal components, F=2 is the free surface amplification, ρ=2.8 g/cm^3 is the density, and v_S = 3.3 km/sec is the estimated average shear-wave velocity in the source region. R_0=5 km represents the reference distance, M_0 denotes the seismic moment, and f_C is the corner frequency. Finally, we compute stress drop estimates from the moment and corner frequencies following Hanks and Thatcher (1972):

$$\Delta\sigma = 8.5 \cdot M_0 \cdot \left(\frac{f_C}{v_S}\right)^3 . \quad (6)$$

The ω^2 fits to the inverted source spectra are indicated in Figure 7a as dashed green lines, showing that the source spectra can satisfactorily be explained using the ω^2-model. Figure 7b shows corner frequency plotted versus seismic moment (on a log-log scale), with the regressional errors of fit (obtained when fitting equation (5) to the source spectra) indicated as horizontal respectively vertical error bars. In the case of self-similar scaling,

the relationship $M_0 \propto f_C^{-3}$ holds and the slope of a fitted straight line in Figure 7b should be close to -1/3. Indeed, we note that this is approximately the case, but at the same time, it is clear that the magnitude range under investigation in this article is much too small to draw any general conclusions on this issue. The stress drops derived using equation (6) range between 0.01 and 2 MPa (Figure 7c). While this is still within the bounds generally found for crustal earthquakes (~0.1-100 MPa, e.g. Kanamori, 1994), the values clearly range at the bottom of this range, indicating comparatively low stress drops for the small earthquakes in this area. Since earthquakes with low stress drops radiate only little high-frequency energy as compared with high stress drop events, this observation can also explain the fact that the local magnitude M_L generally underestimates the moment magnitude M_W by about 0.5 magnitude units, but is otherwise approximately linearly correlated with the latter (Figure 7d).

Site response

Based on the local geological conditions, the stations were divided into three groups, depending on whether they are located on alluvial deposits, debris or colluvial deposits, respectively rock. The geologic characteristics of the sites correspond to the following approximate classification: soft soil, stiff soil and rock (Table 2). The GIT horizontal component site response functions are shown in Figure 8 for six exemplary stations, with two stations from each group. As mentioned earlier, station AND3 (not shown in Figure 7) was chosen as the reference site, assuming a site response of unity, irrespective of frequency, since this station is classified as a hard rock site and the H/V ratio is roughly flat and approximately equal to one over the entire analyzed frequency band (Figure 4).

Figure 8 shows that in general the obtained site response functions are well constrained, with only small standard deviations resulting from the bootstrap analysis.

Overall, the rock sites show as expected lower values of the site response functions over the entire frequency band than stiff and soft soil sites, with no evident predominant frequency peaks. However, it can be clearly seen that also stations located on rock outcrops are not completely devoid of amplification effects (e.g. station VDS3), which may be linked to the weathered and fractured nature of the surface layers and to the shear-wave velocity gradient (e.g. Theodulidis and Bard, 1995; Steidl et al., 1996). On the other hand, stations classified as soft soil and stiff soil generally show more prominent amplification effects, with amplification peaks at some given distinct frequencies (e.g. 4-5 Hz at station CLT3, 8 Hz at station PGN3). The most significant amplification effects were obtained at station CMP3, attaining a factor of about 14 at frequencies of about 8 and 12 Hz.

We also carried out a GIT inversion for the vertical (Z) component using the same S-wave windows as chosen for the horizontal (H) one, and in order to corroborate the site amplification functions obtained from the inversion, we calculated the H/V ratios directly from the observed ground motion spectra as well. For the Z component GIT inversion, we used the same reference condition as for the H component, i.e. the site response at station AND3 is set to unity, irrespective of frequency.

Figure 9 shows the comparison of the GIT H/Z ratio (i.e. the horizontal-to-vertical ratio of the GIT site response functions, solid black line) and the H/V ratios (solid black line with circles) for the same six stations as depicted in Figure 8. The individual GIT site amplification functions for the H (same as shown in Figure 8) and Z components are indicated as well (grey lines with inverted triangles and squares, respectively). A first observation is that the GIT H/Z ratio can satisfactorily explain the main features observed in the H/V ratios (see for instance the peak at 4-5 Hz for station CLT3), with some discrepancies only at low frequencies. These discrepancies may be linked to the fact that,

due to the reference condition, the GIT H/Z ratio at station AND3 is equal to unity, while at the lowest frequencies, the H/V ratio observed at station AND3 starts to rise to about a factor of two. Therefore, it is expectable that the GIT H/Z ratios slightly underestimate the H/V ratios at low frequencies.

Another striking observation is given by the fact that the GIT site response function of the Z component shows remarkable amplification effects for some stations (e.g. CMP3), with the maximum of amplification shifted to higher frequencies as compared with the H component. In such cases, the H/V ratio shows significant differences with the GIT H amplification function, and as Parolai and Richwalski (2004) showed, this effect can be linked to S-P conversions at the bottom of the soft layer in the case of high-impedance contrasts, leading to a reduction of the H/V amplitude due to the amplification of the vertical component at frequencies higher than the fundamental one. Such high-frequency amplification effects on the GIT Z component could also result if significant direct P-wave energy is included in the chosen S-wave windows. This situation could occur if, by selecting a time windows starting 1 sec before the S-wave onset, some late compressional phases with significant amplitudes compared to the high-frequency S-wave part, or in the worst case at stations close to the considered source, the entire P-wave arrival were included the S-wave signal window. This effect is however not expected to be significant in our case, since the hypocentral distances are always larger than 5 km (which roughly corresponds to a minimum S-P travel time difference of 1 sec for typical upper crustal P-wave velocities), with most data points obtained at hypocentral distances of 10 km or larger. Furthermore, in the framework of the GIT methodology, the separation of source spectra and site response relies on a set of records sampling different distances for each earthquake and station. Finally, for stations showing only little amplification of the Z

component (e.g. CLT3 or CSG3), the H/V ratio provides an acceptable first order approximation to the GIT H site response.

DISCUSSION AND CONCLUSIONS

Using the non-parametric GIT approach, we have investigated attenuation characteristics, source spectra, and site response functions for the ISNet seismic network, proving a means to better understand the influence of these different effects on ground motion amplitudes.

We have determined non-parametric attenuation functions for 40 discrete frequencies between 1 and 30 Hz. These functions generally show a relatively simple shape, with a slight change in the rate of amplitude decay between 20 and 50 km. The quality factor Q based on the S-wave part of the recordings shows a pronounced frequency-dependence (close to linear), given by $Q(f) = 28.3 f^{0.87}$. This S-wave attenuation model differs from the results of other authors reported for neighboring regions (Rovelli *et al.*, 1988; Malagnini *et al.*, 2000; Bianco et al., 2002), and in particular shows a less severe frequency-dependence than the results derived by Castro et al. (2004b, 2008) for southern Italy. However, as stated above, it is important to keep in mind that the comparison of different models is complicated by the fact that the data used to estimate them sample different frequency bands and different crustal volumes. Nevertheless, the differences in Q estimates over the range of different studies and regions under investigation indicate that a significant lateral variability in seismic attenuation characteristics exists in Italy. Indeed, Zolezzi et al. (2008), performing an attenuation tomography study of the southern Apennines, showed for instance that the attenuation structure clearly differs on the Tyrrhenian side with respect to the Adriatic side of the southern Apennines chain.

The earthquake spectra corrected for attenuation were used to derive source parameters following the ω^2-model (Brune, 1970, 1971), since the inverted source spectra can be well explained with the ω^2 spectral shape. The obtained corner frequencies and seismic moments provide indications that at least in the narrow magnitude range under investigation, self-similar scaling seems to hold almost perfectly. However, we acknowledge that of course the magnitude range M_L=1.5-3.1 is by far to small to speculate upon any general scaling characteristics of earthquakes in the region. The stress drops range from 0.01 to about 2 MPa, which is close to the lower bounds typically observed for crustal earthquakes (0.1-100 MPa, e.g. Kanamori, 1994). Thus, the earthquakes under investigation in this study seem to show only rather weak high-frequency energy radiation. This conclusion is also compatible with the observation that the local magnitude M_L seems to systematically underestimate M_W by about 0.5 magnitude units.

Finally, the results of the spectral inversion and the H/V analysis point out that only few stations of the ISNet network are not noticeably affected by site effects. Such stations are, as expected, located on rock sites. In addition, some stations located on what appears to be competent rock show amplification in the high frequency range. This could be explained by taking into account the effect of a near-surface, low-velocity layer due to the presence of weathered rock, but also topographic effects might play a role. However, the unfortunately rather poor knowledge of the geologic units below the stations does not allow for any definitive conclusion, and in order to better understand how the observed amplification effects are caused in detail, geotechnical information of subsurface structure is required.

As we have shown, the maximum amplification is generally shifted to higher frequencies in the Z component as compared with the H component, and in some cases, significant amplification effects are visible on the Z component. In such cases, S-P

conversions at the bottom of the soft layer could explain the simultaneously observed reduction of the H/V amplitude due to this amplification on the Z component at frequencies higher than the fundamental one, causing an increased disagreement between the GIT H site response and H/V ratio function. Summarizing our site response results, we can hence state that our observations are in good agreement with previous studies, in particular also with respect to the comparison of GIT and H/V site response estimates (e.g., Field and Jacob, 1995; Bonilla et al., 1997; Parolai et al., 2004), which have shown that the H/V method provides a good estimate of the fundamental frequency of resonance of S-waves, but often underestimates the level of amplification with respect to the GIT approach.

On the basis of our findings, we finally conclude that the results presented in this study allow for an improved characterization of the seismic recordings obtained by the ISNet network. This characterization is of particular importance since the data streams recorded by the ISNet network are intended for usage in real-time seismic information systems (i.e., early warning and near real-time shake map estimation, Iannaconne et al., 2010), and our results provide a means to incorporate knowledge of the attenuation structure, site effects modifying ground motions at the ISNet stations as well as potential correction factors in magnitude estimation into these systems.

ACKNOWLEGMENTS

The data used in this study were recorded by ISNet (Irpinia Seismic Network) managed by Amra Scarl (Analisi e Monitoraggio del Rischio Ambientale) and are available online through http://isnet.na.infn.it/. Data availability is subject to registration. Some of the figures were drawn with the software Generic Mapping Tools (www.soest.hawaii.edu/gmt). This work was performed during a three months visit of L. Cantore at the GFZ German Research Centre for Geosciences in Potsdam, Germany, in the framework of a DAAD (Deutscher Akademischer Austausch Dienst) grant. We would like to thank Marco Mucciarelli and an anonymous reviewer for constructive comments that helped to improve the manuscript.

REFERENCES

Anderson, J. and S. Hough (1984). A model for the shape of the Fourier amplitude spectrum of acceleration at high frequencies. Bull Seism. Soc. Am. 74, 1969-1993.

Andrews, D. J. (1986). Objective determination of source parameters and similarity of earthquakes of different size. Geophysical Monographs 37, 6, 259-267.

Bianco, F., E. Del Pezzo, M. Castellano, J. Ibanez, and F. Di Luccio (2002). Separation of intrinsic and scattering seismic attenuation in the Southern Apennine zone, Italy. Geophys. J. Int. 150 10–22.

Bernard, P., and A. Zollo (1989). The Irpinia (Italy) 1980 earthquake: Detailed analysis of a complex normal faulting, J. Geophys. Res. B94, 1631–1647.

Bonilla, L. F., J. H. Steidl, G. T. Lindley, A. G. Tumarkin, and R. J. Archuleta (1997). Site amplification in the San Fernando Valley, California: variability of site-effect estimation using the S-wave, coda and H/V methods. Bull. Seismol. Soc. Am. 87, 710–730.

Brune, J. N. (1970). Tectonic stress and the spectra of seismic shear waves from earthquakes. J. Geophys. Res. 75, 4997-5009.

Brune, J.N. (1971). Correction. J. Geophys. Res. *76*, 5002.

Castro, R. R., J. G. Anderson, and S. K. Singh (1990). Site response, attenuation and source spectra of S waves along the Guerrero, Mexico, subduction zone. Bull. Seismol. Soc. Am. 80, 1481–1503.

Castro, R. R., F. Pacor, D. Bindi, G. Franceschina and L. Luzi (2004a): Site response of strong motion stations in the Umbria, Central Italy, Region. Bull. Seismol. Soc. Am. **94** (2), 576-590.

Castro, R. R., M.R. Gallipolli and M. Mucciarelli (2004b): An attenuation study in Southern Italy using local and regional earthquakes recorded by seismic network of Basilicata. Annals of Geophys. **47**(5), 1597-1608.

Castro, R.R., M.R. Gallipoli, and M. Mucciarelli (2008). Crustal Q in Southern Italy determined from regional earthquakes. Tectonophysics 457, 96-101.

Cinti, F. R., L. Faenza, W. Marzocchi, and P. Montone (2004). Probability map of the next M ≥ 5.5 earthquakes in Italy. Geochemistry, Geophysics, Geosystem, 5, Q 11003, doi: 10.1029/2004GC000724.

Convertito, V., R. De Matteis, L. Cantore, A. Zollo and G. Iannaccone (2009). Rapid estimation of ground-shaking maps for seismic emergency management in the Campania region of Southern Italy. Natural Hazards, doi: 10.1007/s11069-009-9359-2.

Efron, B., and R. J. Tibshirani (1994). An Introduction to the Bootstrap. Chapman and Hall, London.

Emolo, A., G. Iannaccone, A. Zollo, and A. Gorini (2004). Inferences on the source mechanisms of the 1930 Irpinia (southern Italy) earthquake from simulations of the kinematic rupture process. Ann. Geophys. 47, 1743–1754.

Field, E. H., and K. H. Jacob (1995). A comparision and test of various site-response estimation techniques, including three that are not refernce-site dependent. Bull. Seism. Soc. Am. 4, 1127-1143.

Hanks, T.C., and Thatcher, W. (1972). A graphical representation of seismic source parameters. J. Geophys. Res., 77(23), 4393-4405.

Iannaccone, G., Zollo, A., Elia, L., Convertito, V., Satriano, C., Martino, C., Festa, G., Lancieri, M., Bobbio, A., Stabile, T., Vassallo, M., and Emolo, A. (2010). A prototype system for earthquake early-warning and alert management in southern Italy. Bull. Earthq. Eng. 8, 1105-1129, doi:10.1007/s10518-009-9131-8.

Kanamori, H. (1994). Mechanics of earthquakes, Ann. Rev. Earth Planet. Sci. 22, 207–237.

Konno, K., and T. Ohmachi (1998). Ground-motion characteristics estimated from spectral ratio between horizontal and vertical components of microtremor. Bull. Seismol. Soc. Am. 88, 228–241.

Langston, C. A. (1979). Structure under Mount Rainier, Washington, inferred from teleseismic body waves. J. Geophys. Res. 84, 4749-4762.

Lermo, J., and F. J. Chavez-Garcia (1993). Site effect evaluation using spectral ratios with only one station. Bull. Seism. Soc. Am. 83, 1574-1594.

Malagnini, L., R. B. Herrmann and M. Di Bona (2000). Ground-motion scaling in the Apennines (Italy). Bull. Seismol. Soc. Am., **90** (4), 1062-1081.

Menke, W. (1989). Geophysical Data Analysis: Discrete Inverse Theory, International

Geophysics Series, Academic Press, New York.

Montone, P., M. T. Mariucci, S. Pondrelli, and A. Amato, (2004). An improved stress map for Italy surrounding regions (central Mediterranean). J. Geophys. Res. 109, B10410, doi: 10.1029/2003JB002703.

Nakamura, Y. (1989). A method for dynamic characteristics estimations of subsurface using microtremors on the ground surface. Q. Rep. Railway Tech. Res. Inst. Japan, 30, 25-33.

Oth, A., D. Bindi, S. Parolai, and F. Wenzel (2008). S-wave attenuation characteristics beneath the Vrancea region in Romania: new insights from the inversion of ground-motion spectra. Bull. Seismol. Soc. Am. 98, no. 5, 2482–2497, doi: 10.1785/0120080106.

Oth, A., Parolai, S., Bindi, D., and Wenzel, F. (2009). Source spectra and site response from S waves of intermediate-depth Vrancea, Romania, earthquakes. Bull. Seismol. Soc. Am. *99*, 235-254, doi: 10.1785/0120080059.

Pantosti, D., and G. Valensise (1990). Faulting mechanism and complexity of the 23 November 1980, Campania-Lucania earthquake, inferred from surface observations. J. Geophys. Res. 95, 15319–15341.

Parolai, S., D. Bindi, and P. Augliera (2000). Application of the generalized inversion technique (GIT) to a microzonation study: numerical simulations and comparison with different site-estimation techniques. Bull. Seismol. Soc. Am. 90, 286–297.

Parolai, S., and S. M. Richwalski (2004). The importance of converted waves in comparing H/V and RSM site response estimates. Bull. Seismol. Soc. Am. 94, 304–313.

Parolai, S., D. Bindi, M. Baumbach, H. Grosser, C. Milkereit, S. Karakisa, and S. Zünbül

(2004). Comparison of different site response estimation techniques using aftershocks of the 1999 Izmit earthquake. Bull. Seismol. Soc. Am. 94, 1096–1108.

Rovelli, A., O. Bonamassa, M. Cocco, M. Di Bona and S. Mazza (1988). Scaling laws and spectral parameters of the ground motion in active extensional areas in Italy. Bull. Seismol. Soc. Am., 78 (2), 530-560.

Steidl, J., A. G. Tumarkin, and R. J. Archuleta (1996). What is a reference site? Bull. Seism. Soc. Am. 86, 1733-1748.

Theodulidis, N. and Bard, P.-Y. (1995). Horizontal to vertical spectral ratio and geological conditions: an analysis of strong motion data from Greece and Taiwan. Soil. Dyn. Earthquake Eng., 14,177–197.

Weber, E., V. Convertito, G. Iannaccone, A. Zollo, A. Bobbio, L. Cantore, M. Corciulo, M. Di Crosta, L. Elia, C. Martino, A. Romeo, and C. Satriano (2007). An advanced seismic network in the southern Apennines (Italy) for seismicity investigations and experimentation with earthquake early warning. Seism. Res. Lett. 78, 622–534.

Westaway, R. (1987). The Campania, southern Italy, earthquakes of 1962 August 21. Geophys. J. R. Astr. Soc. 8, 1–24.

Westaway, R., and J. Jackson (1987). The earthquake of 1980 November 23 in Campania-Basilicata (southern Italy). Geophys. J. R. Astr. Soc. 90, 375–443.

Zolezzi, F., P. Morasca, K. Mayeda, W. S. Phillips, and C. Eva (2008). Attenuation tomography of the Southern Apennines (Italy). J. Seismol. 12, 355–365.

TABLES

Table 1: S-wave attenuation models reported for Italy

Region	Frequency range (Hz)	Q-model	Geometrical spreading	Reference
Central and Central-southern Apennines	$0.1 \leq f \leq 20$	$Q(f) = 100\ f$	$1/r$	Rovelli et al. (1988)
Entire Apennines	$0.24 \leq f \leq 5.0$	$Q(f) = 130\ f^{0.1}$	$r^{-0.9}$, $r \leq 30$ km r^{0}, $30 \leq r \leq 80$ km $r^{-0.5}$, $r \geq 80$ km	Malagnini et al. (2000)
Umbria-Marche	$0.3 \leq f \leq 9.5$	$Q(f) = 31.2\ f^{1.2}$	$1/r$	Castro et al. (2004a)
Southern Italy	$1.6 \leq f \leq 10$	$Q(f) = 32.1\ f^{1.7}$	$10/r^{b}$ $b=1.0\pm0.2$	Castro et al. (2004b)
Irpinia-Basilicata (southern Italy)	$1 \leq f \leq 30$	$Q(f) = 28.3\ f^{0.87}$	$5/r$ (reference distance 5 km)	This study

Table 2: List of stations with the respective geological underground classification

CGG3	stiff soil
LIO3	stiff soil
CMP3	stiff soil
TEO3	stiff soil
CLT3	soft soil
RDM3	stiff soil
COL3	stiff soil
SCL3	stiff soil
CSG3	rock
PST3	stiff soil
SNR3	rock
AND3	rock
VDP3	stiff soil
STN3	rock
NSC3	rock
PGN3	stiff soil
SRN3	soft soil
VDS3	rock
BEL3	soft soil
RSF3	stiff soil
AVG3	rock
MNT3	stiff soil

FIGURE CAPTIONS

Figure 1. Stations of the ISNet seismic network used in this work. Station symbols and color code indicate the geological site classification: grey circles indicate rock, black triangles stiff soil and open squares soft soil sites (see also Table 2). The solid black lines represent the surface projection of the three fault segments that ruptured during the 23 November 1980 earthquake (M 6.9).

Figure 2. Station locations (triangles), traces of fault segments (solid black lines), and source-station paths (grey lines) of the considered dataset. Two cross-sections through the epicentral area (one with latitude, one with longitude) are depicted as well.

Figure 3. a) Local magnitude M_L versus hypocentral distance R distribution for the dataset used in the inversion. b) Number of events with given M_L for the dataset used in the inversion.

Figure 4. Average H/V ratio calculated at station AND3. The grey-shaded area indicates the standard deviation. Note the approximately flat shape, with a slight rise above a value of 2 only at low frequencies.

Figure 5. a) Non-parametric attenuation functions (distance range 5-83 km) at 40 frequencies (1-30 Hz) obtained in the first step of the inversion scheme. The functions are color-coded with respect to the corresponding frequency (see legend). b) Two of the attenuation functions depicted in a) with their respective standard deviation from bootstrap analysis indicated as grey-shaded areas.

Figure 6. *Q(f)* model derived from the analysis of the non-parametric attenuation functions shown in Figure 5 (solid black line). Dots and error bars indicate the individual Q-values obtained at each considered frequency, and the solid black line represents the fit to these

data points of the form $Q(f)=Q_0 f^N$. Other models from the literature are indicated in their frequency range of validity (overlapping with our frequency range) for comparison (see text).

Figure 7. Source results obtained from the spectral inversion. a) All source spectra (in acceleration) as derived from the GIT inversion at a reference distance of R_0=5 km, color-coded with respect to their M_L values. Green dashed lines indicate ω^2 model fits. b) Corner frequency versus seismic moment plot. The grey line indicates a log-linear fit, with a slope close to the expected theoretical value of -1/3 in the case of self-similar scaling. c) Stress drop values computed as given in equation (6). d) Local magnitude M_L versus moment magnitude M_W as estimated from the spectral fits shown in a). Note that M_L systematically underestimates M_W by about 0.5 magnitude units.

Figure 8. Calculated GIT site response functions for six stations. The solid line indicates the mean with the grey-shaded area depicting the standard deviation of 200 bootstrap samples. The top panels are examples for stations classified as rock sites (see Table 2), while the middle and bottom panels relate to stations classified as stiff and soft soil, respectively.

Figure 9. Comparison of H/V ratios calculated directly from the ground motion spectra (black lines with circles) and the GIT H/Z ratios (i.e. GIT site response on H component divided by GIT site response on Z, black solid lines) for the same six stations as depicted in Figure 8. The individual GIT site response functions for horizontal and vertical component are indicated as well with grey lines with inverse triangles and squares, respectively.

FIGURES

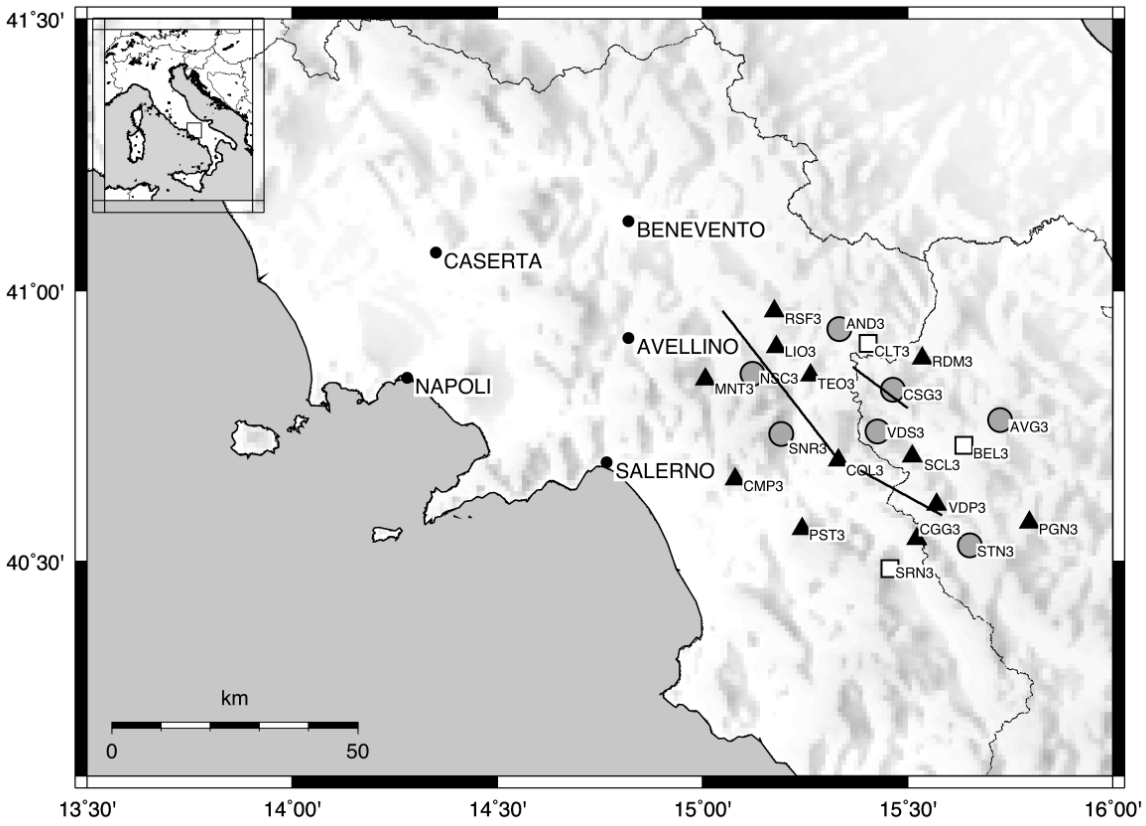

Figure 1

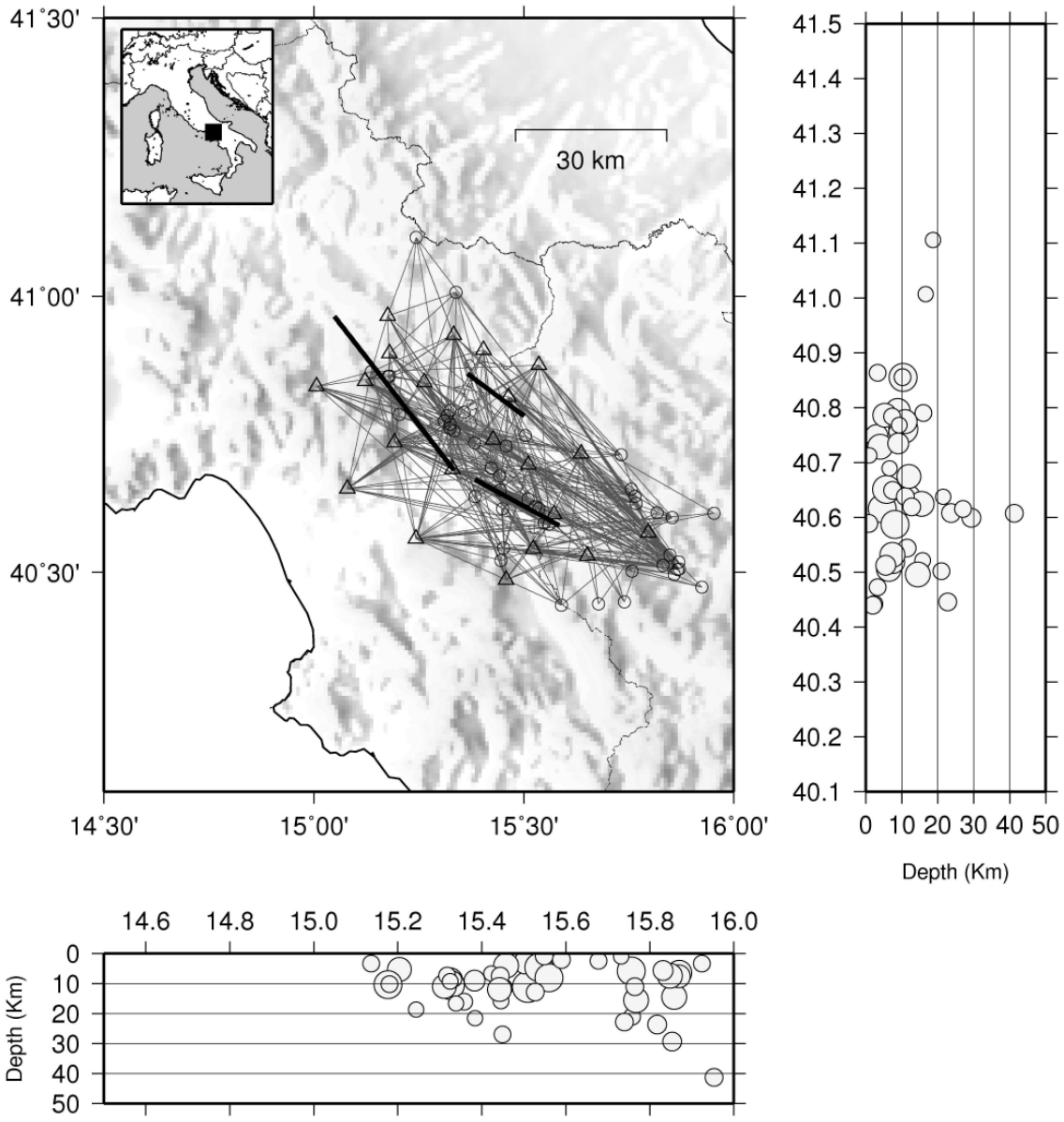
41°30'
41°00'
40°30'
14°30'
15°00'
15°30'
16°00'
30 km
41.5
41.4
41.3
41.2
41.1
41.0
40.9
40.8
40.7
40.6
40.5
40.4
40.3
40.2
40.1
0 10 20 30 40 50
Depth (Km)
14.6 14.8 15.0 15.2 15.4 15.6 15.8 16.0
0
10
20
30
40
50
Depth (Km)

Figure 2

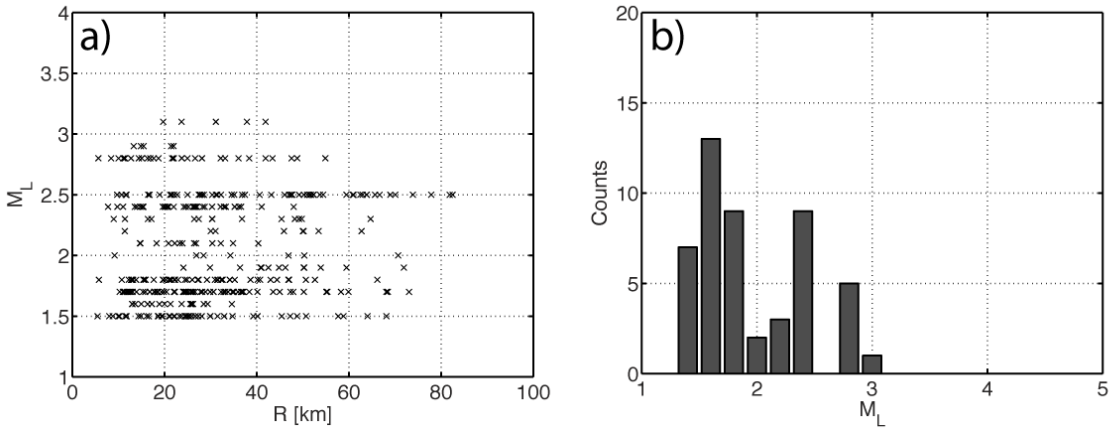

Figure 3

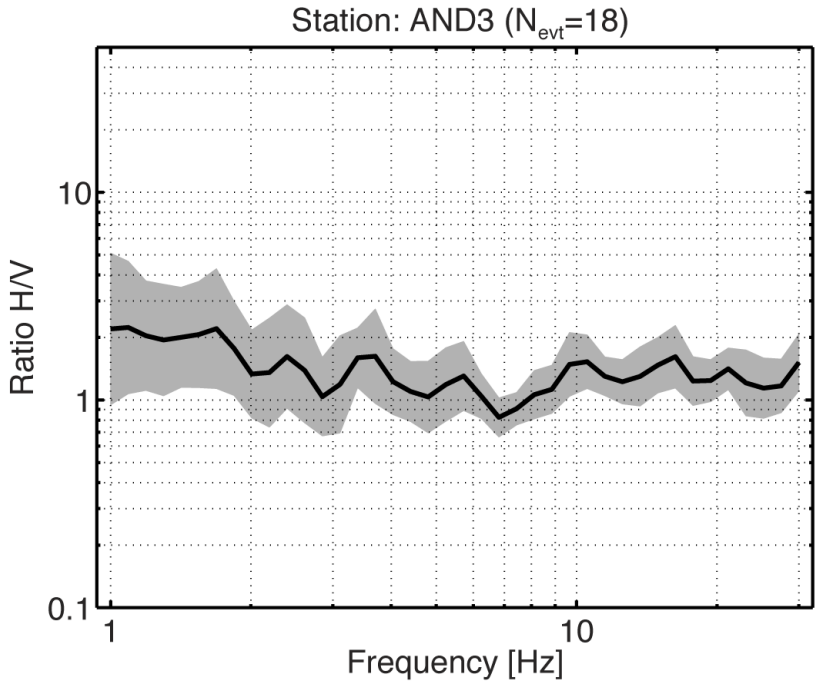

Figure 4

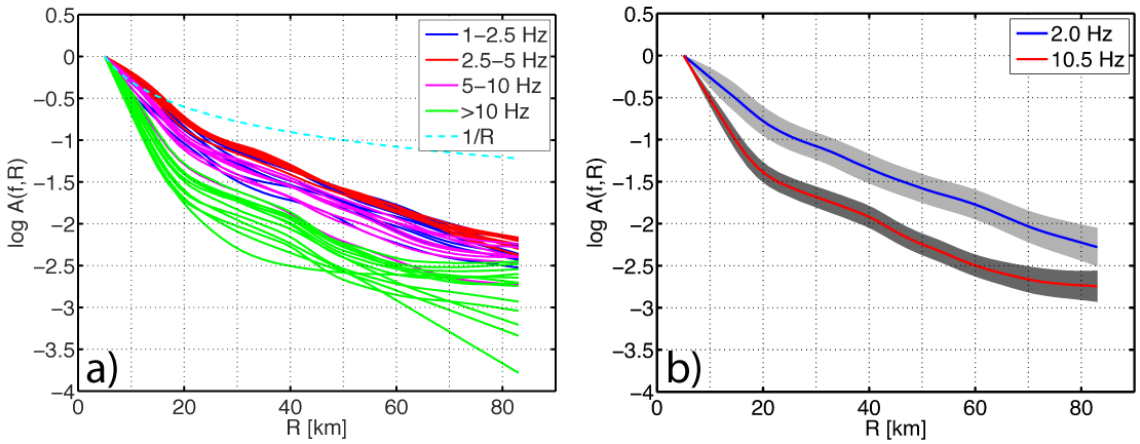

Figure 5

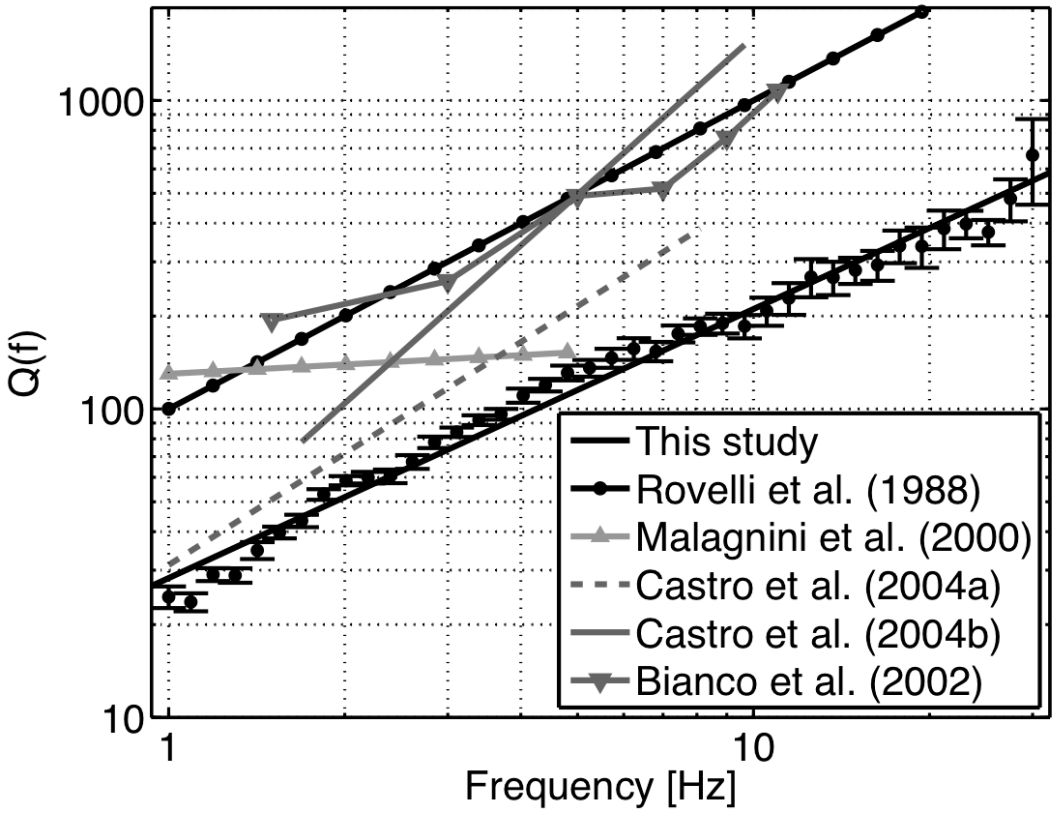

Figure 6

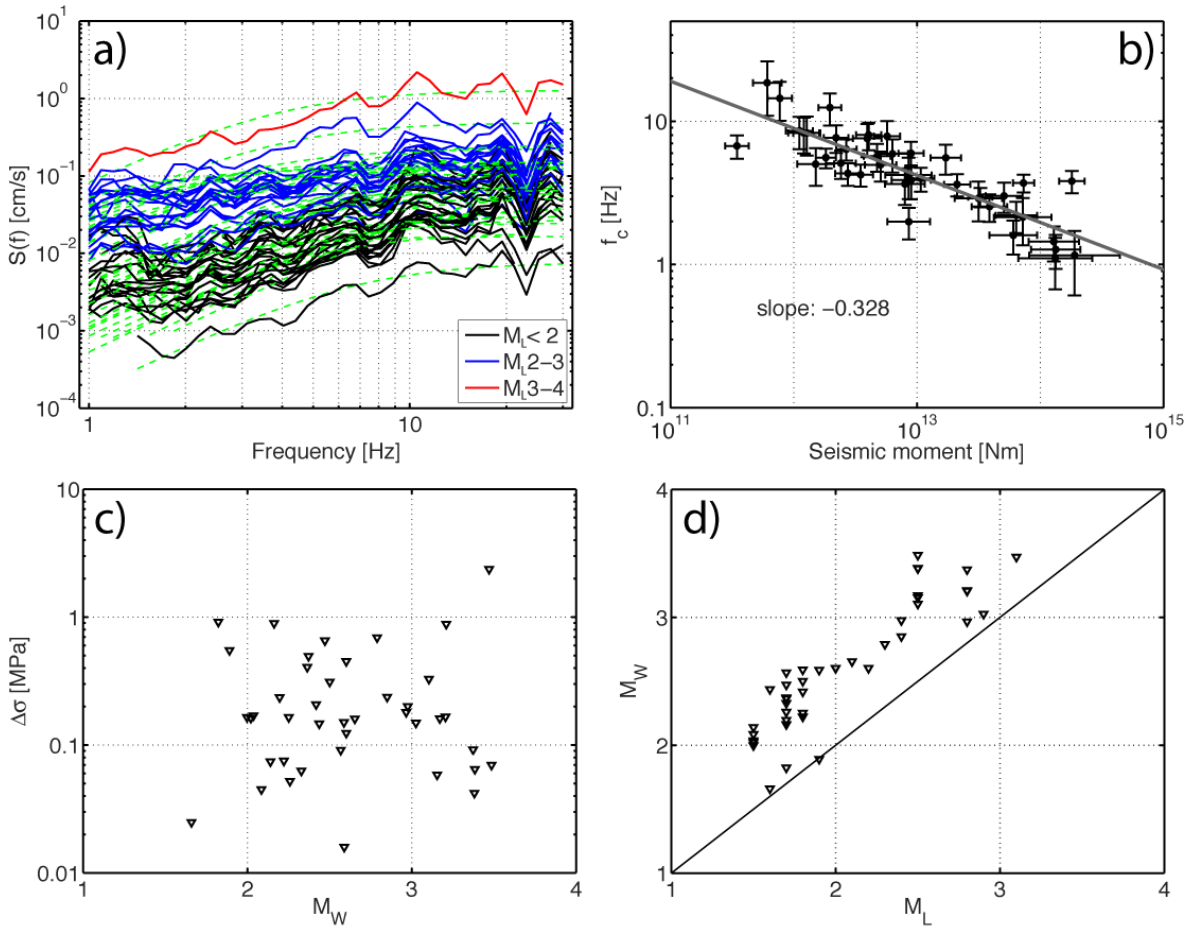
a)
S(f) [cm/s]
Frequency [Hz]
M_L< 2
M_L2–3
M_L3–4
b)
f_c [Hz]
slope: −0.328
Seismic moment [Nm]
c)
Δσ [MPa]
M_W
d)
M_W
M_L

Figure 7

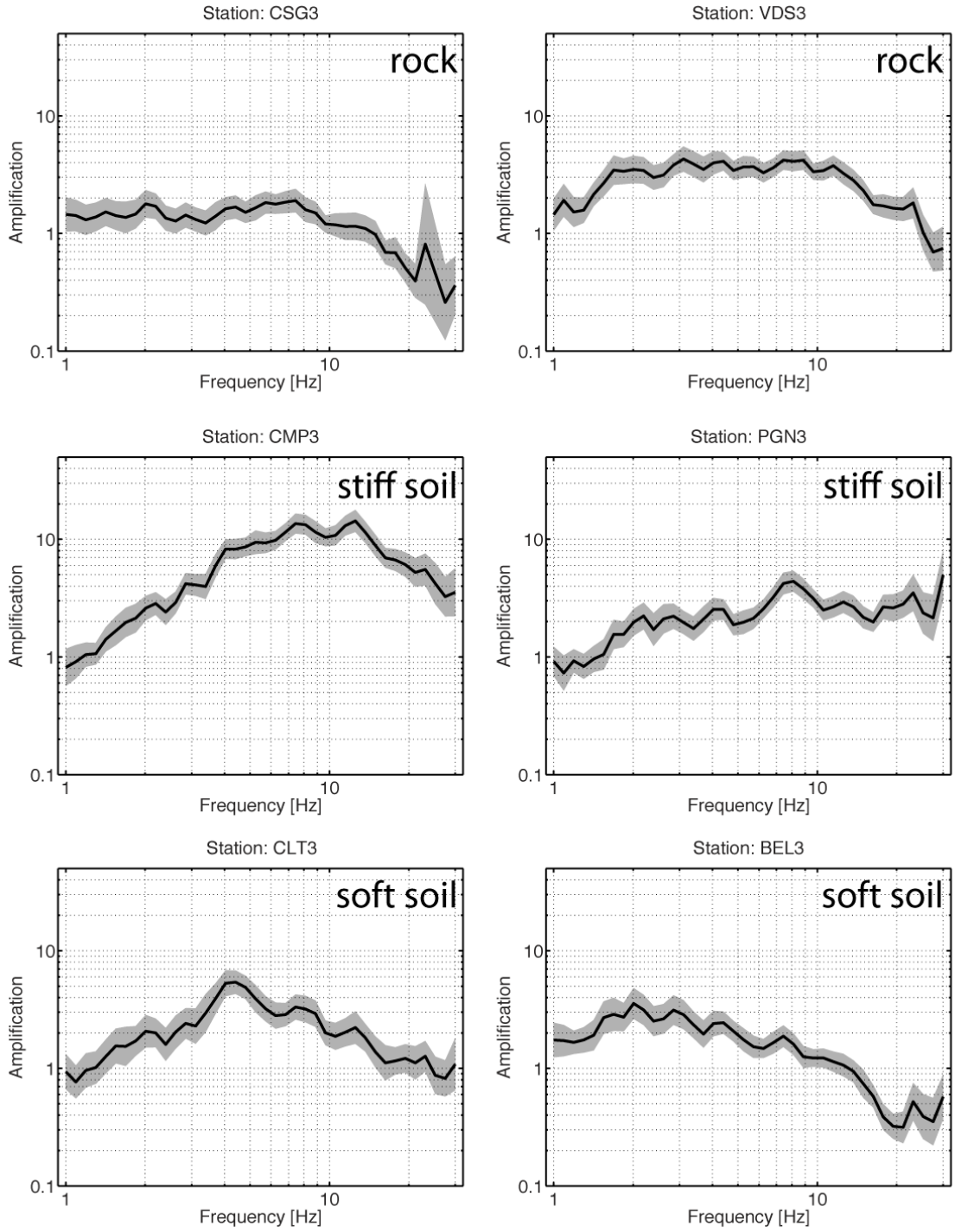
Station: CSG3
rock
Station: VDS3
rock
Station: CMP3
stiff soil
Station: PGN3
stiff soil
Station: CLT3
soft soil
Station: BEL3
soft soil
Amplification
Frequency [Hz]
0.1
1
10

Figure 8

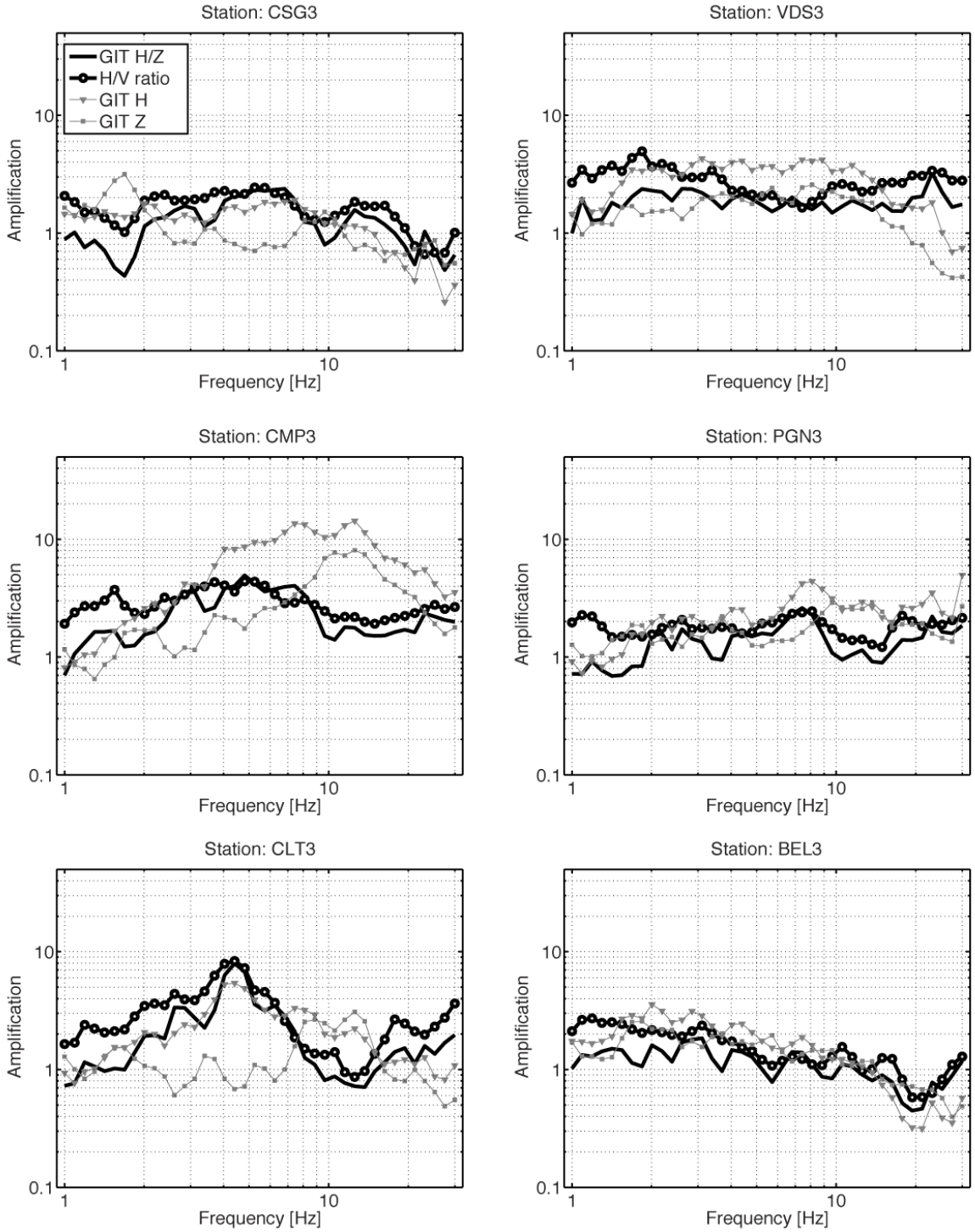
Station: CSG3
GIT H/Z
H/V ratio
GIT H
GIT Z
Station: VDS3
Station: CMP3
Station: PGN3
Station: CLT3
Station: BEL3
Amplification
Frequency [Hz]
0.1
1
10

Figure 9